


# Additive manufacturing of individual bone implants made of bioresorbable calcium phosphate cement using the example of large skull defects

Stefan Holtzhausen , Philipp Sembdner, Martin Pendzik,  
Holger Wilhelm Rudolf Schmidt and Kristin Paetzold-Byhain

Technische Universität Dresden, Germany

 stefan.holtzhausen@tu-dresden.de

## Abstract

In the field of individualized medical implants for bone replacement, additive manufacturing offers far-reaching advantages for bridging bone defects and supporting the production of natural form and function. The article uses the example of a large, customized cranial implant to show the challenges of manufacturing with osteoinductive bone cements. The process is shown, starting with planning and design, through to functional integration using adapted manufacturing strategies to create defined porosity.

*Keywords: 3D printing, biomedical design, functional modelling, case study, technology development*

## 1. Introduction

Additive manufacturing processes allow the production of complex and filigree components with simultaneous functional integration (Du Plessis *et al.*, 2019). Particularly in the field of individual medical implants for bone replacement, additive manufacturing offers significant advantages in this respect in order to bridge bone defects and support the recreation of natural form and function (Haleem *et al.*, 2020). The targeted integration of lattice structures or cellular structures with different porosities (Muallah *et al.*, 2021; Hendrikson *et al.*, 2017) can be used to stimulate bone growth in a targeted manner. Until now, the integration of these osteoconductive properties is only possible with additive manufacturing processes. Furthermore, the use of bioactive materials can stimulate bone resorption and thus enable the complete formation of new bone in defect areas that vary in shape and size.

Calcium phosphate cement (CPC) is an established material with these osteoinductive properties (Lindner *et al.*, 2014). This synthetic material imitates the inorganic part of human bone. Material properties such as paste-like consistency, biocompatibility and the biodegradability make CPC structures ideal substrates for various cells. Since CPC also has an osteoconductive effect, i.e. it acts as a kind of guide rail for cells, it is ideal for use in the field of bone regeneration (Xu *et al.*, 2017; Kinne *et al.*, 2021). CPC is currently used for the cemented anchoring of implants, whereby the material is applied in a paste-like state and then hardens. There are also a few manufacturers who produce CPC in prefabricated blocks of different sizes using additive manufacturing (Heinemann *et al.*, 2013). The individual implant shape is only realized intraoperatively by adapting it to the defect site.

In general, the goal should be to create bone replacement structures tailored to each patient prior to implantation, thereby minimizing surgical time. Besides precise planning and modeling an accurate additive manufacturing is essential for achieving this goal. However, due to the pasty nature of CPC material during processing, specific requirements must be considered, especially concerning pre-

processing and support structure design. This is particularly important when printing non-planar individual shapes with varying porosities to facilitate targeted bone ingrowth.

This paper presents a pre-processing procedure for additive manufacturing of customized bone replacement structures from pasty CPC material. It demonstrates the necessary interfaces with planning and design and showcases the usability of the procedure through a case study on the production of large-scale customized cranial implants.

## 2. Fundamentals

### 2.1. CPC and current additive processing

The CPC material used (Figure 1) is provided by the company INNOTERE GmbH (Radebeul, Germany). The CPC consists of cement powder components (calcium hydrogen phosphate ( $\alpha$ -Ca<sub>3</sub>(PO<sub>4</sub>)<sub>2</sub>), calcium carbonate (CaCO<sub>3</sub>), precipitated hydroxyapatite (Ca<sub>10</sub>(PO<sub>4</sub>)<sub>6</sub>(OH)<sub>2</sub>) and finely ground potassium hydrogen phosphate (K<sub>2</sub>HPO<sub>4</sub>). The components are mixed and achieve a paste-like consistency through the addition of a carrier liquid. (Reitmaier *et al.*, 2018; Ahlfeld *et al.*, 2017)

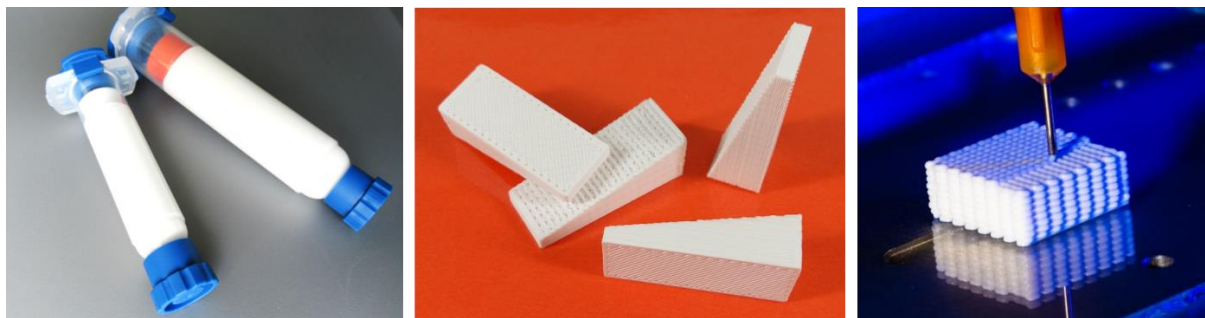


**Figure 1. CPC paste and blocks and 3D printing of planar CPC structures (company INNOTERE)**

Due to its paste-like consistency, CPC can be processed using extrusion-based, additive manufacturing processes, known as direct writing (ISO/ASTM 52900). Scaffolds made of CPC are usually additively manufactured in layers with orthogonally alternating orientation at 0° and 90° or at -45° and 45° (Muallah *et al.*, 2021; Korn *et al.*, 2020). The CPC is in a viscous state and is printed by means of air pressure from a material cartridge directed vertically downwards through a defined extrusion needle onto a base or a shaping negative (Reitmaier *et al.*, 2018). Currently, flat glass plates are often used as a base or pastes as a support structure in the form of a sacrificial ink material (Korn *et al.*, 2020; Ahlfeld *et al.*, 2018). The disadvantage of previous methods is that either no individual non-planar shape can be reproduced or that 3D printers with several cartridges are required to process different materials, whereby the sacrificial ink material must also be washed out afterwards. Studies have shown that cell settlement is favored by greater path spacing and thus greater porosity (approx. 60% to 70%) (Muallah *et al.*, 2021). The material remains pasty during printing and hardens over several days at high humidity.

The applications of CPC for customized implants are manifold. For example, CPC has been used for the production of patient-specific hybrid cranial implants, bone replacement structures in the jaw area and osteochondral bone replacement structures in combination with hydrogels as cartilage replacements (Muallah *et al.*, 2021; Kilian *et al.*, 2021). This shows the increasing medical need for additively manufactured individual implants made from bioresorbable, bioactive materials such as CPC.

### 2.2. Entire process for producing individual implants

The work in this paper is based on a process consisting primarily of six steps, which has been established for the development of customized medical implants (Pendzik *et al.*, 2021; Schulz *et al.*, 2023). The process chain primarily takes into account data acquisition, data preparation, planning, design, pre-processing and manufacturing (Figure 2).

The digital process begins with the acquisition and determination of patient-specific data (e.g. using CT) during data collection. In the subsequent data processing, this CT data is segmented and discrete 3D models of the tissue area being considered are extracted. In the planning phase, the design of the implant is then developed in close cooperation with the attending physician depending on the position, the patient-specific conditions and other boundary conditions. In the modeling phase, the implant is designed virtually with all its functions and properties. The models are then prepared in pre-processing according to the material used, the manufacturing process and the requirements for the defect site, e.g. using slicing processes in additive manufacturing, and the manufacturing parameters are defined. Finally, the implant is manufactured, which includes the production of the implant body itself and corresponding post-processing steps (e.g. removal of support material, polishing of contact surfaces).

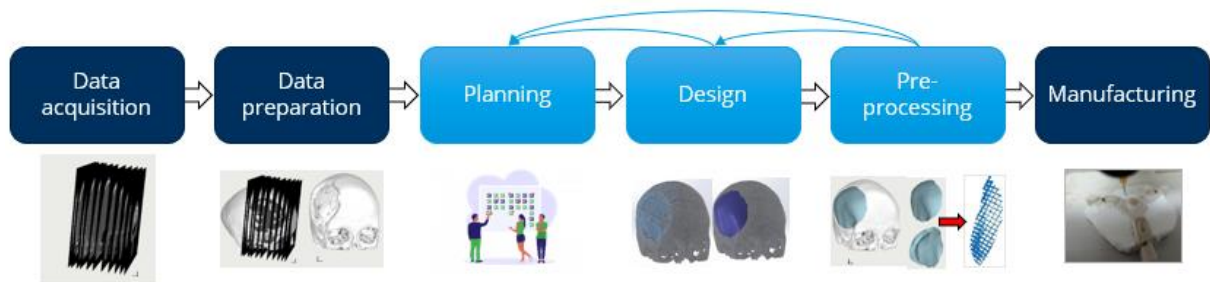


Figure 2. Process chain for the manufacture of customized medical implants

### 3. Pre-processing methods for printing individual implants from CPC

#### 3.1. Challenges and research question

In the additive manufacturing of individual bone implants from CPC, several challenges arise. Firstly, there's the material behavior during printing, which necessitates meticulous pre-processing involving defined production strategies and optimal production parameters. Additionally, ensuring that the individual bone implant precisely matches the shape of the area to be replaced and maintains true-to-shape contact surfaces with the remaining bone presents another hurdle. To achieve this, efficient support mechanisms like support plates must be developed to accurately replicate the individual shape. Moreover, achieving targeted bone ingrowth requires realizing several density phases through adjustable porosity in the bone replacement structure (Figure 3). This serves to mimic natural bone composition, with densely printed areas featuring low porosity resembling the solid, load-bearing cortical layer, and less dense areas imitating the spongy, cancellous regions. Adjusting these porosity levels is crucial for facilitating optimum bone growth.

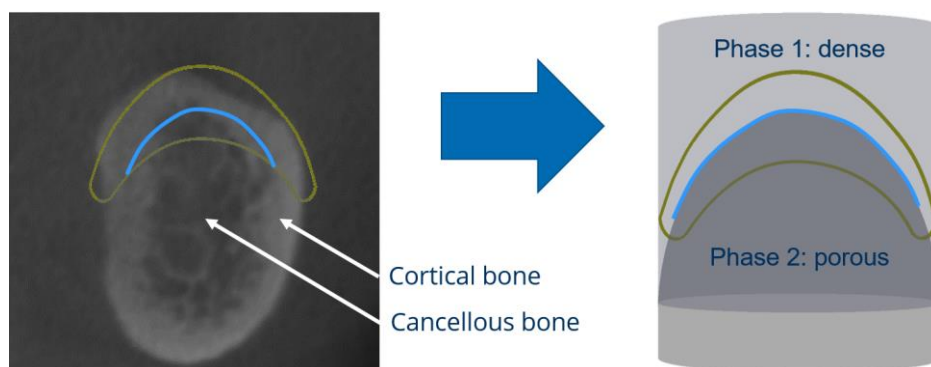


Figure 3. Left: CT cross-section (blue - border between bone types, yellow - replacing area); right: two density phases and individual outer implant shape (yellow) (Sembdner *et al.*, 2023)

In this respect the following research question arises: How can pre-processing procedures for additive manufacturing of customized bone replacement structures from pasty CPC material be optimized to address the challenges associated with material behavior, shape accuracy and porosity control, ultimately enhancing bone ingrowth and implant performance? The research question is answered taking into account the process chain described in chapter 2.2. by presenting pre-processing methods and their dependence on planning and design information (shown in blue in Figure 2).

### 3.2. Data provision from planning and design

The interface between planning, implant design and pre-processing is particularly relevant for the realization of optimal biomechanical and functional properties of the individual implant. The CTinA (*CT in Application*) method for processing imaging data and providing planning as well as design information (Hofmann *et al.*, 2018), which was developed at the Chair of Virtual Product Development (TU Dresden), is used in this work for data provision. The method allows efficient visualization of the imaging data. The methodology is based on approaches from reverse engineering. The core of the procedure are methods for the problem-specific representation and processing of discrete volume data. Relevant information for product development is extracted and automatically converted into a form of representation suitable for further steps in the product development process. For example, during development, reference geometries can be used to retrieve information on local image information. Additionally, image processing methods are employed to automatically extract information through techniques such as edge detection, among others.

With this method, all data and information relevant for production can be transferred to pre-processing. On the one hand, this includes the implant's external geometry based on the patient's individual bone situation. The CTinA process makes the assisted design of the implant possible using all available information from imaging data. Furthermore, functional elements such as drill holes, handle pockets, etc. can be integrated. These are necessary for pre-processing to map the exact geometry. On the other hand, design restrictions such as the maximum possible angle or bevels must be taken into account to prevent a collision of the needle, for example. In a next step, medically relevant areas, contact surfaces to soft tissue, osseointegrative layers, etc., which must have a specific porosity, have also be defined in planning and design process. This is possible using separate geometry elements, so-called masks.

As a result, the respective geometry elements of the envelope geometry and areas with the same porosity as well as the corresponding meta information (e.g. porosity to be achieved from imaging data) are available for subsequent production. The final geometric mapping of the porosity is carried out in pre-processing. The geometries are transferred in the form of a discrete, surface-describing triangular mesh (\*.stl; \*.3mf; \*.obj) or in the form of open CAD formats (\*.stp).

### 3.3. Development of printing strategies and associated parameters including a support structure

Production is carried out using the already established direct writing process (ISO/ASTM 52900). The basis for this is the extrusion of the CPC via a defined needle, which is attached to the lower part of the material cartridge (Figure 1 right). The usual diameters are 250  $\mu\text{m}$ , 330  $\mu\text{m}$  and 410  $\mu\text{m}$ . There are other sizes, but these do not play a role in the intended application. It should be noted, however, that needle blockages often occur at a needle diameter of 250  $\mu\text{m}$ , which is why smaller diameters can be ruled out. The diameter of the needle, the speed of the extruder and the extrusion pressure applied to the cartridge determine the size of the extruded strand. Based on previous work (Muallah *et al.*, 2021), these parameters can be limited to 330  $\mu\text{m}$  and 410  $\mu\text{m}$  needle diameter, approx. 3 - 5 bar extrusion pressure and 250 to 500 mm/min, whereby the result is also influenced by the ambient and storage conditions of the paste. The strand diameter to be achieved determines the geometric resolution of the printed body. Elements that are smaller than the strand diameter, e.g. very thin wall sections, are not mapped. As a result, even standard pores cannot be printed if they have been directly modeled in the geometry transferred from the design (see classic metal implants with a cellular structure in Figure 4 left). As a result, pores can only be achieved through the spatial structure of the deposited strand (Figure 4 right).

Implant in Ti6Al4V

Bone-Scaffold in CPC

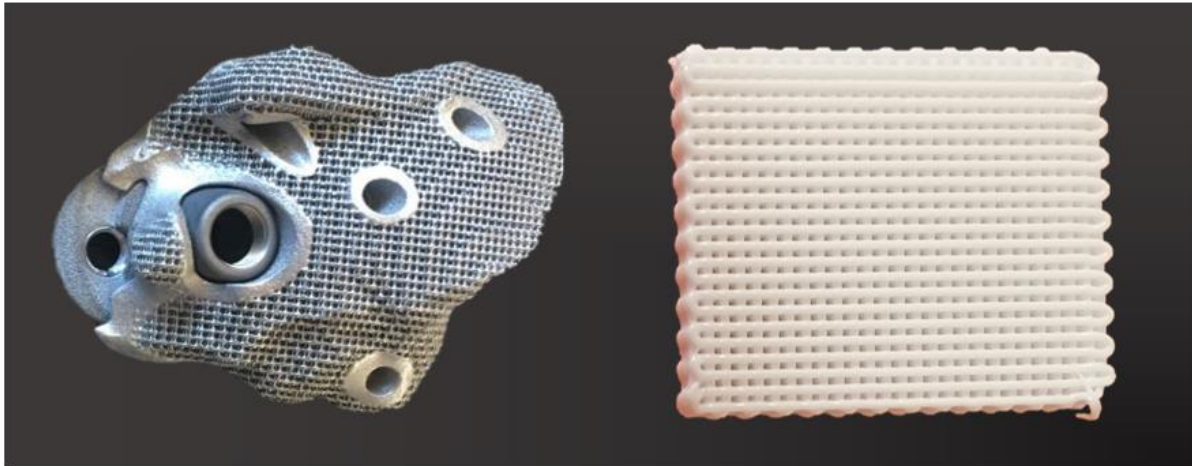


**Figure 4. Different representation of the porous structure due to different materials and manufacturing processes**

After transferring the data from the design process, the print direction is defined. This should preferably be selected in such a way that there are as few overhang areas as possible. Furthermore, application-related criteria as well as the material itself play an important role in the orientation of the component. As already described, the material remains pasty during printing and therefore tends to slip due to gravity. As a result, the implants should be positioned appropriately flat to reduce the built-up weight. It may also be necessary to produce individual surfaces to a particularly high quality. Here it has been shown that the surface in contact with the printing platform are reproduced more accurately (Figure 5).

Top-Side

Bottom-Side

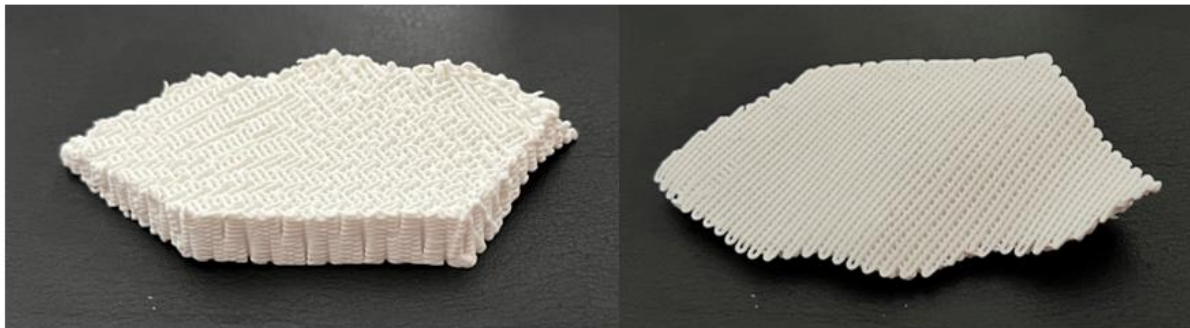


**Figure 5. Additive manufactured CPC scaffold; left: clearly wavy surface in printing direction; right: true-to-shape surface on the side of the printing platform**

After aligning the component in the printing direction, the slicing and subsequent calculation of the contour paths and the filling pattern takes place. The layer spacing can be calculated as a function of the needle diameter, whereby values of approx. 75 % of the diameter are particularly suitable. Established strategies based on the meandering structure within a layer have established themselves as filling strategies. An orientation and a defined path spacing are specified. The path spacing is essential for the achievable porosities. Usable parameters (path spacing 950  $\mu\text{m}$  needle  $\text{\O}$  410  $\mu\text{m}$ ) have already been identified for the ingrowth of cells (Muallah *et al.*, 2021; Holtzhausen *et al.*, 2020). In the process presented here, the mask objects (see section 3.2), which are also cut at the appropriate height, are also taken into account when calculating the filling pattern. These contours are offset against the cutting contour of the implant using boolean operations (Figure 6). As the mask geometries define areas that

are to be printed without porosity, a path distance of 550  $\mu\text{m}$  (needle  $\text{\O} 410 \mu\text{m}$ ) has been established here.

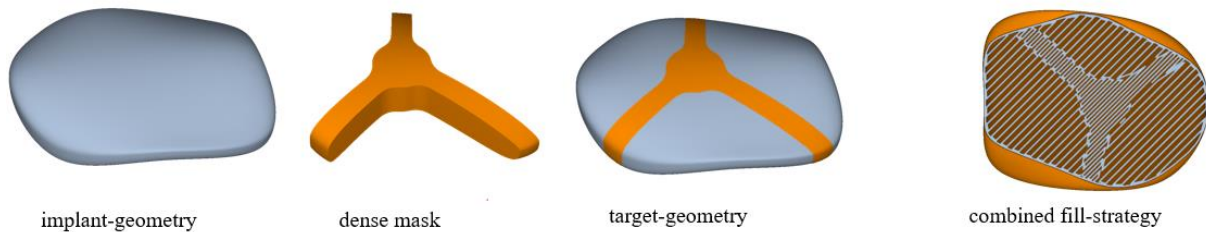


**Figure 6. Implant-geometry, dense mask and target geometry for calculation of manufacturing pathes in combined fill-strategy**

Usually, free-form objects need to be supported during printing. Processes from the plastics or metal sector calculate these support structures based on the model geometry and manufacture them from the same material. These structures are then removed in a post-process step. Due to the pasty consistency of the material, this process cannot be used with CPC. Separately manufactured support structures made of biocompatible plastic are used here (Figure 7). Referencing in the building space is carried out using geometric landmark geometries (planes, body edges), which allow the coordinate transformation of the support structure and the manufacturing coordinate system (Holtzhausen *et al.*, 2019).

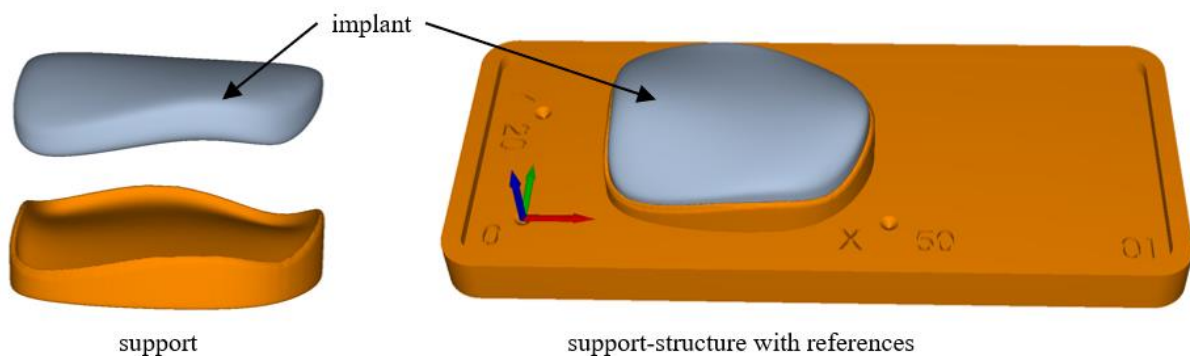


**Figure 7. Calculated support plate made of biocompatible plastic using 3D printing**

Figure 8 shows the individual steps of the pre-processing-phase described above. All information regarding geometry, including the defined porosity, as well as all information on the dispensing needle used from the previous process steps (Figure 2) Design and Planning are available as input. An extension of the manufacturing process presented is the deformation of the printed paths in such a way that they follow the shape of the support structure. The starting point for this is the support geometry that has already been created. Instead of calculating planar cutting planes, an offset geometry is calculated iteratively from the support structure. To make the process robust, signed distance fields (Bærentzen and Aanaes, 2002) are used instead of surface-describing triangular meshes. Based on the underlying voxel description, which stores the signed distances to the object surface, offset surfaces can be calculated by simple addition operations within the field. This is followed by the calculation of the spatial intersection curve with the implant geometry. To calculate the paths, this spatial curve is projected into the building plane, where the meandering paths are calculated as described above, and then projected back onto the offset surface. As a result, the manufacturing paths are not in the usual layered, planar form, but in a form that follows the support structure. As a result of the pre-processing, manufacturing paths are available in \*.gcode or \*.nc format, which are readable for the manufacturing system. The support structures geometries are also available in the form of \*.stl files and can be additively manufactured from a biocompatible plastic.

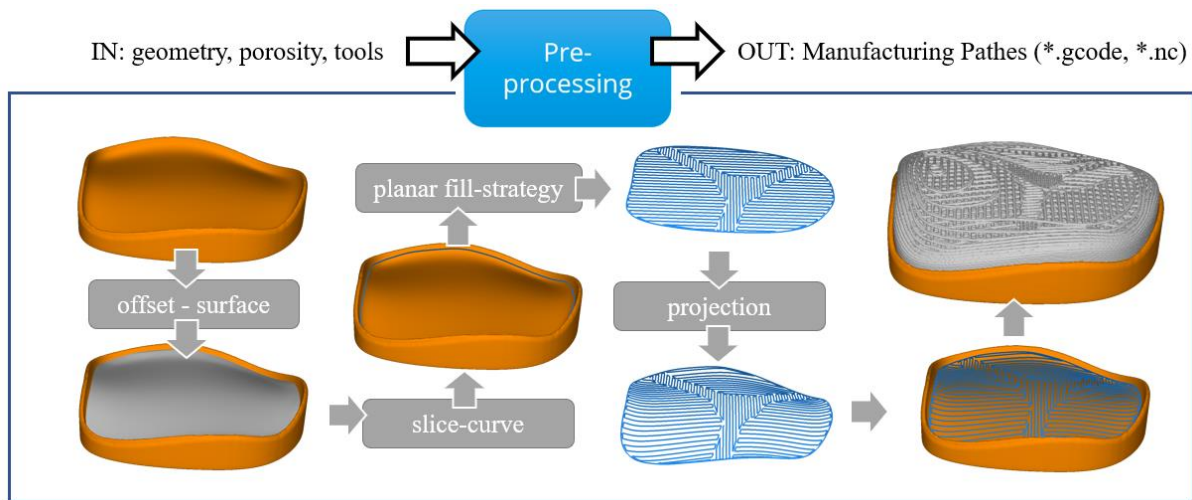


Figure 8. Calculation of the shape-following and two-phase path geometries based on the implant geometry and the calculated support structure

#### 4. Case study for the application of the pre-processing method

The previous chapter 3 described the possibilities for influencing the configuration and layout of a customized implant in the process steps of planning, design and pre-processing. In the following, the development process will be examined on the basis of a case study, taking into account the newly developed pre-processing step. The aim is to comprehensively test the process from data preparation to manufacturing and to verify whether the type of pre-processing presented fits into the established development process. A large-scale skull defect serves as a case study. Using the example of a large skull defect, the following section shows how a customized implant can be designed using the aforementioned options and taking into account the material and defect-specific boundary conditions. The added value of the skull defect as a case study example is based on the fact that this defect is very complex due to its size, its curvature as well as the different widths of the marginal contour and the varying thickness of the bone. Furthermore, the design of large-area implants made of CPC is particularly difficult due to the fragile material behavior. Initial approaches to solving this problem demonstrate the realization of hybrid implant designs with a correspondingly load-bearing and bioactive material structure (Penzik et al., 2023). Such a large defect therefore requires a load-bearing structure, which makes the implementation of a multiphase structure necessary. A further challenge in this context is a possible upgrade of the implant in the sense of functional integration in order to ensure that the implant can be adapted, especially for growing children. Considering the modeling effort and the requirements of the defect site, this case study can be classified as very complex in the context of individual implants. The high complexity of this case study therefore allows a reliable statement on the transferability to other defects.

##### 4.1. Development of an individual implant using the example of a cranial defect

###### Cranial defect and requirements

An example of application is a cranial defect located on the side of the neurocranium (brain skull). The defect affects the *Os frontale* (frontal bone), the *Os parietale* (parietal bone), the *Os sphenoidale* (sphenoid bone) and the *Os temporale* (temporal bone). It has a circumference of approx. 324 mm at the outer edge. The inner edge measures 276 mm. Figure 9 shows the defect and the two edges in the CTinA software environment. The particular complexity of this defect lies both in its size and in its distribution over four areas of the cranial bone. The latter leads on the one hand to a multidirectional and therefore very complicated edge contour. On the other hand, the different bone areas have different bone thicknesses. These range from 2 mm to 10 mm. Both aspects significantly complicate and influence both the implant design and manufacturing. The size of the defect plays a major role in that such a large

implant made of CPC cannot be manufactured in one piece. One reason for this is the pasty manufacturing state of the CPC, which sets the boundary conditions for manufacturing, e.g. with regard to weight and curvature. Another reason is that a larger contact surface between the CPC and the shaping negative results in a stronger adhesion between these two. As a result, the larger the contact is, the bigger is the challenge of removing the cured CPC implant from the negative without destroying it. Another key aspect of such a large defect is the ability to adapt to the patient's growth if necessary. This cannot be taken into account with an implant consisting of just one element. The division of the implant into several elements is therefore advisable and expedient for several reasons.

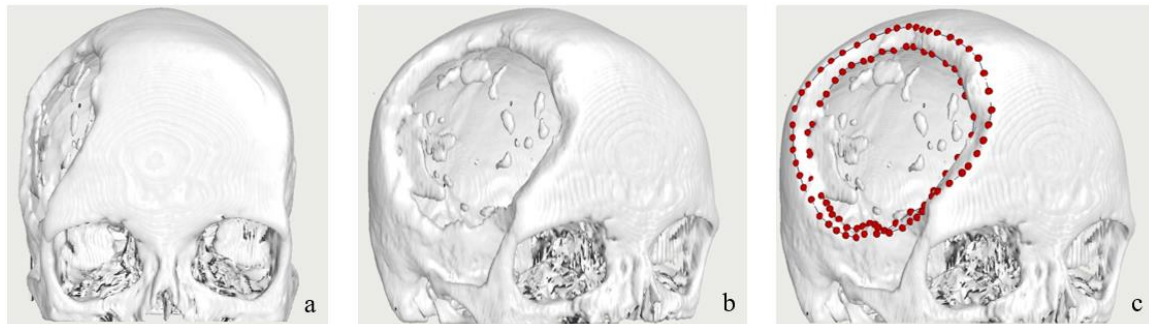


**Figure 9.** Lateral cranial defect (a: frontal; b: 45°; c: 45° view with outer and inner edge)

## Modeling

The raw implant model is modeled according to Pendzik et al. (Pendzik et al., 2023). First, the defect site is modeled. Several splines are placed around the region of interest (Figure 10a and Figure 10b), from which a closed surface is generated in several steps and finally a solid of the defect site is created. Based on this model, guiding lines are used (Figure 10c), which lie close to the contour of the missing bone, to derive the boundary surfaces of the raw implant model, in this case the outer surface of the skull. The raw model of the implant with surface functions and Boolean operations is generated analogous to the defect site. Figure 10d, Figure 10e and Figure 10f show the designed raw model of the individual implant.

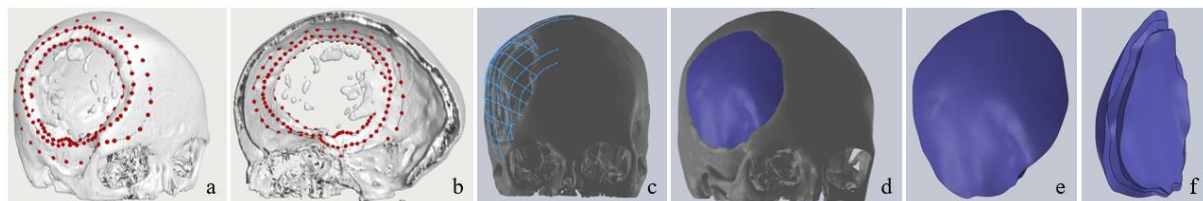


**Figure 10.** Modeling steps from the CT data to the raw implant model (a and b: splines for defect site modelling; c: Auxiliary lines for modeling the outer surface of the implant; d: raw model of the implant with skull; e and f: raw model of the implant)

In the next step, the raw model is divided into two different dense phases. Figure 11a shows the separation into the dense and thus load-bearing phase (yellow) and the open-porous phase (purple). A centrally positioned, three-arm load-bearing structure is selected. A specifically mechanical and simulation-optimized design of the load-bearing structure was not pursued here, as no valid material model for CPC exists according to the current state of research. The entire model is then divided into its elements according to the selected splitting option (Figure 11b). On the one hand, the *separating contour* for the separation of the raw model into the respective individual elements must be selected. In this case, the snake shape is used as the separating contour, which is shown in Figure 11c. In addition to the separating contour, the type or shape of the cut itself is also relevant. Potential variants are, for example, a smooth cut or an S-shaped cut. The S-shape was favored as the *cutting contour* for the cross-section for this implant (Figure 11d). Both the snake shape as a dividing contour and the S-shape as a cutting contour are better suited for a strong connection with the strongly curved and large defect. Due to the chosen contours, the entire structure may shift apart as desired, but will not fall apart or slip out of place.



The orange lines represent the cutting contour on the outer surface of the implant model, the blue lines the cutting contour on the inner surface. Both contours are connected via the S-shape. The individual elements were each designed with a contact area between the shaping negative and the element of less than 1,600 mm<sup>2</sup> for easy removal from the negative. The upper limit was set at 2,000 mm<sup>2</sup>. Furthermore, 14 cylindrical holes were placed in such a way that the CPC elements can be connected to each other and to the skull bone using biocompatible sutures (Figures Figure 11d and Figure 11e).

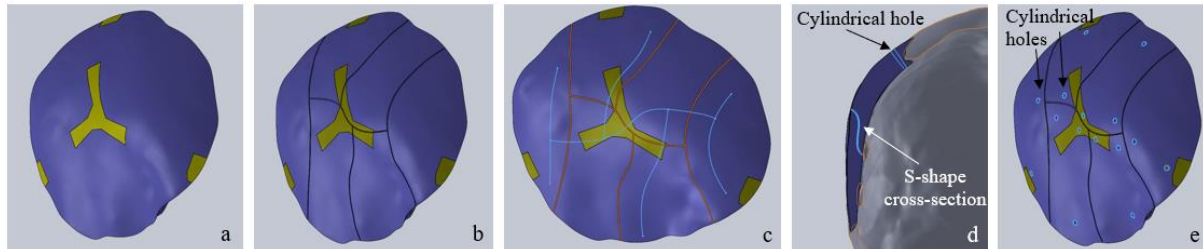


**Figure 11. Design of the individual elements of the raw implant model (a: separation into dense and open porous phase; b: separation into individual elements; c: Lines in serpentine form for the separating contour (orange: outside, blue: inside); d: Sectional view with cylindrical hole and S-shaped section between two elements; e: Individual parts with cylindrical holes)**

### Pre-processing and Manufacturing

The manufacturing paths are calculated as described above. A support structure was calculated for each element and manufactured in the material PC-ISO on a Stratasys Vantage system using the FDM process. The individual implant elements are printed as a paste-like CPC in the shaping negative of the support structures. For this purpose, for each element the shaping negative is used to divide the implant element into curved layers (compare to Figure 8) and the manufacturing parameters such as path spacing are set according to the requirements. A path spacing of 550  $\mu\text{m}$  was selected for the dense areas.

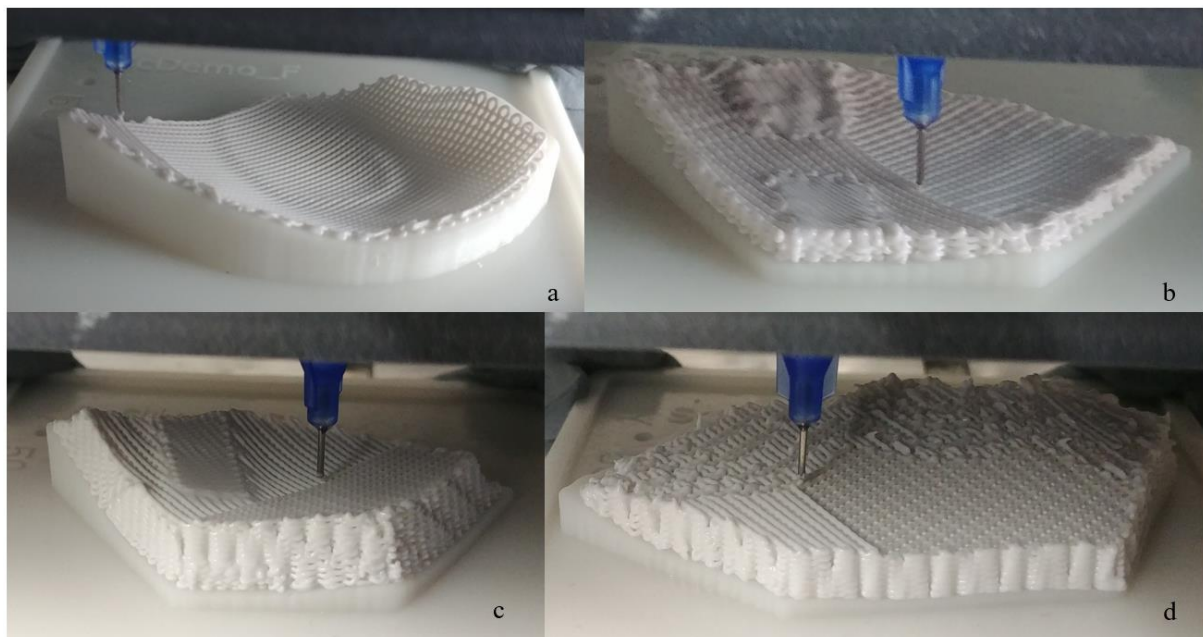


**Figure 12. Manufacturing of the individual CPC elements (a: Element F - start of third layer; b: Element C - fourth layer with different density phases; c: Element C - close to the end of manufacturing with different density phases; d: Element D - close to the end of manufacturing)**

With a needle diameter of 410  $\mu\text{m}$ , the layer spacing is just as large. The path spacing of the open porous areas is 950  $\mu\text{m}$ . This achieves a sufficiently large porosity, which favors cell growth. An extrusion pressure of 3 bar and a feed rate of 250 mm/min are used for all elements. Figure 12a clearly shows

manufacturing close to the contour. Figures 12b and 12c, on the other hand, show the manufacturing of different phases within a layer.

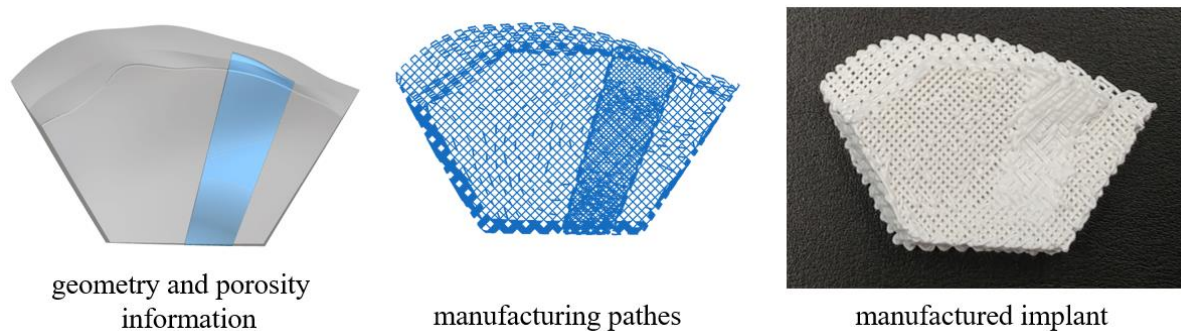


**Figure 13. Overview of the process steps based on a segment of the planned implant**

Figure 13 shows the implementation of two-phase CPC parts for an individual segment of the implant, starting with planning and design information for the geometry and the necessary various dense phases, through the corresponding manufacturing paths to the manufactured and cured implant part.

## 4.2. Results

Based on the application example, the individual implant was manufactured from CPC in six individual parts. The process shown here was closely followed. However, the model was simplified for the first manufacturing trial in order to be able to guarantee full manufacturability for the demonstrator. Specifically, a honeycomb shape was selected as the separating contour, the cutting shape for the cross-section was simplified and the cylindrical holes provided for connecting the individual parts were removed. The functional version of the implant, shown in Figure 11e, will be manufactured in future trials. As can be seen in Figure 14a, all CPC elements of the implant were successfully manufactured. Both the dense and the open porous phases are clearly visible. Despite the large height of 10 mm in some cases, hardly any sagging of the structure was observed. All CPC elements could be removed very well from the shaping negative, regardless of the shape and thickness. Flat areas in particular are often difficult or impossible to remove non-destructively. It was also found that the central element required a total of two more days to cure - one in air humidity and one in a water bath - than the usual six days for CPC structures - three in air humidity and three in a water bath. However, this is the element with the largest volume of dense phase. Figures Figure 14b to Figure 14d show both the individual elements and the large individual implant assembled from them.

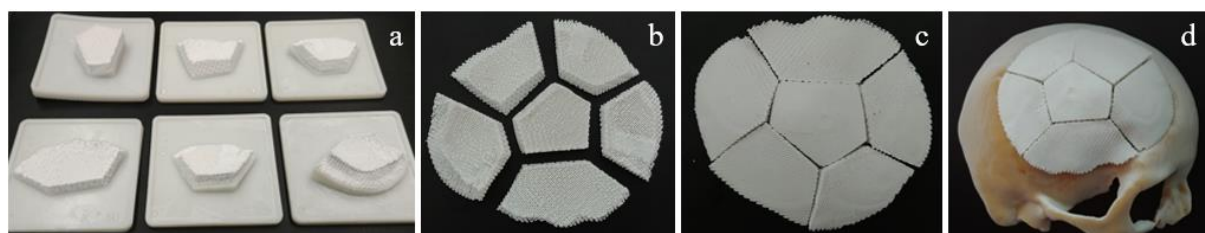


**Figure 14. Manufactured individual implant consisting of 6 individual parts (a: with shaping negative; b: individual; c: assembled; d: inserted in the demonstrator skull)**

## 5. Discussion

The paper shows the possibilities of pre-processing in the manufacture of implants made of CPC. In particular, the adaptation of the local pore size as well as the novel, shape-following orientation of the production paths contributes significantly to extending the process limits in the production with CPC. The functional customization possibilities of the designer increase through the integration of different porosities within its construction. At the same time the example presented was able to show in concrete terms how an individual implant made of CPC can be developed, designed and manufactured. In

particular, the design sequence and the limit value with regard to the maximum size of the contact surface of the individual CPC elements to the shaping negatives proved to be effective. The latter led to a completely non-destructive removal of the individual CPC elements from the support structure. Furthermore, the biological and mechanical properties of the implant could be implemented and influenced, particularly during pre-processing. For example, phases with different densities were successfully produced within a single element. Geometric specifications such as the separation and cutting contour or cylindrical holes were not yet taken into account in the demonstrator. Considerably more frequent setting down of the extrusion needle and considerably more narrow areas in the structure would have been the result if they had been taken into account. However, the elements were simplified in favor of the manufacturability of the first demonstrator. The manufacturability of these more complex structures must be tested in the following steps in order to ensure full functionality and stability in use. It was also noticeable that very dense phases sometimes lead to a longer curing time. The CPC element with the largest proportion of dense phase still had soft areas in the core of the dense phase at the contact surface to the shaping negative even after the standardized six-day curing time. One possible cause is the lack of contact with water in these areas. If the phase is too dense and no longer has any porosity, uniform penetration of the water is no longer guaranteed. Conversely, this means that a purely dense phase should not exist. The result would be areas that do not harden completely on the outside and inside, which can significantly affect both the mechanical and biological properties. Reproducibility is also currently a challenge. Sometimes the smallest air inclusions cause minimal defects in the structure. Especially with low CPC elements, this can already have an influence on cell growth behavior. Another complicating factor is that there are slight differences in viscosity between different CPC batches. The question here is whether and how this can be incorporated into the printing strategy in the future.

## 6. Summary and outlook

In order to enable patient-specific treatment with larger replacement structures based on biologically resorbable, osteoconductive bone cement, further issues must be addressed in the future. The monolithic production of such large implants is challenging due to the fragility and brittleness of the material. The multi-part production described above requires concepts for connecting the elements to each other. The attachment of the structures to the bone also requires fundamental research from a design and medical perspective. The solutions presented also still need to be optimized due to the multi-criteria challenges along the *design - production - medical use* process path. For example, the properties of the material in the printing process play a key role in the design. This includes, for example, running paste due to its own weight, which can close medically relevant pores. Simulation approaches (material models, strength, manufacturing process, biological effectiveness) have not yet been considered. These are the subject of current research work by the authors (Seidler et al., 2023).

## References

- Ahlfeld, T., Akkineni, A.R., Förster, Y., Köhler, T., Knaack, S., Gelinsky, M. and Lode, A. (2017), "Design and Fabrication of Complex Scaffolds for Bone Defect Healing. Combined 3D Plotting of a Calcium Phosphate Cement and a Growth Factor-Loaded Hydrogel", *Annals of Biomedical Engineering*, Vol. 45 No. 1, pp. 224–236, <https://dx.doi.org/10.1007/s10439-016-1685-4>.
- Ahlfeld, T., Köhler, T., Czichy, C., Lode, A. and Gelinsky, M. (2018), "A Methylcellulose Hydrogel as Support for 3D Plotting of Complex Shaped Calcium Phosphate Scaffolds", *Gels (Basel, Switzerland)*, Vol. 4 No. 3, <https://dx.doi.org/10.3390/gels4030068>.
- Bærentzen, A. and Aanæs, H. (2002), "Generating Signed Distance Fields From Triangle Meshes".
- Du Plessis, A., Broeckhoven, C., Yadroitsava, I., Yadroitsev, I., Hands, C.H., Kunju, R. and Bhate, D. (2019), "Beautiful and Functional: A Review of Biomimetic Design in Additive Manufacturing", *Additive Manufacturing*, Vol. 27, pp. 408–427, <https://dx.doi.org/10.1016/j.addma.2019.03.033>.
- Haleem, A., Javaid, M., Khan, R.H. and Suman, R. (2020), "3D printing applications in bone tissue engineering", *Journal of clinical orthopaedics and trauma*, Vol. 11 No. Suppl 1, S118-S124, <https://dx.doi.org/10.1016/j.jcot.2019.12.002>.
- Heinemann, S., Rössler, S., Lemm, M., Ruhnow, M. and Nies, B. (2013), "Properties of injectable ready-to-use calcium phosphate cement based on water-immiscible liquid", *Acta biomaterialia*, Vol. 9 No. 4, pp. 6199–6207, <https://dx.doi.org/10.1016/j.actbio.2012.12.017>.

- Hendrikson, W.J., Deegan, A.J., Yang, Y., van Blitterswijk, C.A., Verdonchot, N., Moroni, L. and Rouwkema, J. (2017), “Influence of Additive Manufactured Scaffold Architecture on the Distribution of Surface Strains and Fluid Flow Shear Stresses and Expected Osteochondral Cell Differentiation”, *Frontiers in bioengineering and biotechnology*, Vol. 5, p. 6, <https://dx.doi.org/10.3389/fbioe.2017.00006>.
- Hofmann, D., Sembdner, P., Holtzhausen, S. and Stelzer, R. (2018), “Approach for using ct data in product development processes”, *The e-Journal of Nondestructive Testing*, Vol.23 No.02.
- Holtzhausen, S., Heinemann, S., Lemm, M. and Stelzer, R. (2019), “Printing of contour-adapted bone scaffolds based on calcium phosphate cements”, *CARS 2019*, <https://dx.doi.org/10.1007/s11548-019-01969-3>.
- Holtzhausen, S., Kilian, D., Sembdner, P., Lode, A., Gelinsky, M. and Stelzer, R. (2020), “Adjustment of locally resolved pore sizes for extrusion printing of biomaterials”, *DDMC2020 - Fraunhofer Direct Digital Manufacturing Conference*, 2020.
- ISO/ASTM 52900, *Additive manufacturing - General principles - Fundamentals and vocabulary*, 2021st ed., International Organization for Standardization, Geneva.
- Kilian, D., Sembdner, P., Bretschneider, H., Ahlfeld, T., Mika, L., Lütznier, J., Holtzhausen, S., Lode, A., Stelzer, R. and Gelinsky, M. (2021), “3D printing of patient-specific implants for osteochondral defects: workflow for an MRI-guided zonal design”, *Bio-Design and Manufacturing*, <https://dx.doi.org/10.1007/s42242-021-00153-4>.
- Kinne, R.W., Gunnella, F., Kunisch, E., Heinemann, S., Nies, B., Maenz, S., Horbert, V., Illerhaus, B., Huber, R., Firkowska-Boden, I., Bossert, J., Jandt, K.D., Sachse, A., Bungartz, M. and Brinkmann, O. (2021), “Performance of Calcium Phosphate Cements in the Augmentation of Sheep Vertebrae-An Ex Vivo Study”, *Materials (Basel, Switzerland)*, Vol. 14 No. 14, <https://dx.doi.org/10.3390/ma14143873>.
- Korn, P., Ahlfeld, T., Lahmeyer, F., Kilian, D., Sembdner, P., Stelzer, R., Pradel, W., Franke, A., Rauner, M., Range, U., Stadlinger, B., Lode, A., Lauer, G. and Gelinsky, M. (2020), “3D Printing of Bone Grafts for Cleft Alveolar Osteoplasty - In vivo Evaluation in a Preclinical Model”, *Frontiers in bioengineering and biotechnology*, Vol. 8, p. 217, <https://dx.doi.org/10.3389/fbioe.2020.00217>.
- Lindner, M., Bergmann, C., Telle, R. and Fischer, H. (2014), “Calcium phosphate scaffolds mimicking the gradient architecture of native long bones”, *Journal of biomedical materials research. Part A*, Vol. 102 No. 10, pp. 3677–3684, <https://dx.doi.org/10.1002/jbm.a.35038>.
- Muallah, D., Sembdner, P., Holtzhausen, S., Meissner, H., Hutsky, A., Ellmann, D., Assmann, A., Schulz, M.C., Lauer, G. and Kroschwald, L.M. (2021), “Adapting the Pore Size of Individual, 3D-Printed CPC Scaffolds in Maxillofacial Surgery”, *Journal of Clinical Medicine*, Vol. 10 No. 12, <https://dx.doi.org/10.3390/jcm10122654>.
- Pendzik, M., Holtzhausen, S., Heinemann, S. and Paetzold, K. (2023), “FURTHER DEVELOPMENT OF THE DESIGN PROCESS FOR HYBRID INDIVIDUAL IMPLANTS”, *Proceedings of the Design Society*, Vol. 3, pp. 2035–2044, <https://dx.doi.org/10.1017/pds.2023.204>.
- Pendzik, M., Mika, L., Scheibner, B., Holtzhausen, S. and Stelzer, R. (2021), “Development of a process for designing hybrid implants for production using additive manufacturing”, *Proceedings of the 32nd Symposium Design for X, DFX 2021*, <https://dx.doi.org/10.35199/dfx2021.18>.
- Reitmaier, S., Kovtun, A., Schuelke, J., Kanter, B., Lemm, M., Hoess, A., Heinemann, S., Nies, B. and Ignatius, A. (2018), “Strontium(II) and mechanical loading additively augment bone formation in calcium phosphate scaffolds”, *Journal of orthopaedic research official publication of the Orthopaedic Research Society*, Vol. 36 No. 1, pp. 106–117, <https://dx.doi.org/10.1002/jor.23623>.
- Schulz, M.C., Holtzhausen, S., Nies, B., Heinemann, S., Muallah, D., Kroschwald, L., Paetzold-Byhain, K., Lauer, G. and Sembdner, P. (2023), “Three-Dimensional Plotted Calcium Phosphate Scaffolds for Bone Defect Augmentation—A New Method for Regeneration”, *Journal of personalized medicine*, Vol. 13 No. 3, p. 464, <https://dx.doi.org/10.3390/jpm13030464>.
- Seidler, A., Pendzik, M., Hilbig, A., Sembdner, P., Holtzhausen, S. and Paetzold-Byhain, K. (2023), “Investigation of manufacturing deviations of CPC scaffolds for improving the design process”, *Current Directions in Biomedical Engineering*, Vol. 9 No. 1, pp. 551–554, <https://dx.doi.org/10.1515/cdbme-2023-1138>.
- Sembdner, P., Pohlmann, H., Wendler, A., Matschke, J.B., Kroschwald, L., Holtzhausen, S., Hutsky, A., Ellmann, D., Lauer, G. and Paetzold, K. (2023), “Approach for Rapid Fabrication of Individual Bone Replacement Structures by Designing Additively Prefabricated CPC Models”, *Lachmayer, Bode et al. (Hg.) 2023 – Innovative Product Development by Additive Manufacturing*, Vol. 2023, pp. 60–75, [https://dx.doi.org/10.1007/978-3-031-27261-5\\_5](https://dx.doi.org/10.1007/978-3-031-27261-5_5).
- Xu, H., Wang, P., Wang, L., Bao, C., Chen, Q., Weir, M.D., Chow, L.C., Zhao, L., Zhou, X. and Reynolds, M.A. (2017), “Calcium phosphate cements for bone engineering and their biological properties”, *Bone Research*, Vol. 5, <https://dx.doi.org/10.1038/boneres.2017.56>.